João Miguel Ramalho Fidalgo Rosa

Licenciatura em Ciências de Engenharia
de Micro e Nanotecnologias

Study of Gold Nanoparticle Assisted Neuron Stimulation

Dissertação para obtenção do Grau de Mestre em
Engenharia de Micro e Nanotecnologias

Orientador: Adam R. Kampff, Principal Investigator, Intelligent Systems Lab

Co-orientador: Elvira Fortunato, Professora Doutora, Faculdade de Ciências e
Tecnologia da Universidade Nova de Lisboa

FACULDADE DE
CIÊNCIAS E TECNOLOGIA
UNIVERSIDADE NOVA DE LISBOA

Setembro 2015

"The brain is a world consisting of a number of unexplored continents and great stretches of unknown territory."

Santiago Ramón y Cajal,

1906 Nobel Prize of Medicine

Acknowledgements

I would like to thank everyone in my life during the long months that separated the time when I first started thinking about the project I wanted to pursue and the time when I wrote these words. It has been a thriving journey: often scary, dangerous and utterly unpredictable at times; but fun, rewarding and exciting nonetheless. There are many people not mentioned here, for which I am deeply sorry, but I know that you'll know who you are.

First of all, I want to thank Joana Neto for the amazing opportunity that these months have presented me: for introducing me to Dr. Adam Kampff and making this dissertation possible, for always being there whenever needed, for never giving up on a seemingly hopeless experiment and for just being a tirelessly wonderful person. Without her, none of these pages would be here.

To Dr. Adam Kampff for the opportunity, guidance, positivity and all the learning experiences his ever-present constructive criticism and novel, practical ideas provided me with.

To Prof. Elvira Fortunato and Prof. Rodrigo Martins for the guidance during the last five years, and for building, in the university, a great network of research, projects and people; without which these pages would also not be here.

To Júlio Costa and Nuno Coelho, who have accompanied me in this journey since the start and up until the very end. Clearly this experience would not have been remotely as good as it was had it not been shared with you guys.

To everyone in the Intelligent Systems Lab, who helped whenever possible and always had something incredibly interesting to talk about. Particularly to George Dimitriadis, who was a great, tireless help during the starting months of research; João Frazão, Pedro Lacerda, Lorenza Calcaterra and Athabak Dehban for the company, fun and support.

To everyone in the Champalimaud Center for the Unknown, particularly those who lended us essential equipment without which this research would not be possible; particularly Niccolò Bonacchi, Rodrigo Dias and Tiago Monteiro.

To everyone at CENIMAT/I3N for always being available to help, even when barely knowing me.

To my family, who made me the person I am today: I'm sorry for all the dinners I've lost because of lasers, gold nanoparticles and writing this document. You've been an invaluable support for all these 23 years.

To my girlfriend, Sofia Jacinto, for keeping me sane, positive and cheerful even in the darkest of times. I suspect that without you, these pages would be much harder.

To my close friends, both from my hometown and from university: Tiago Pestana, Cátia Costa, Diogo Vaz, Afonso Ferreira, João Jacinto, Rui Carreiras, Raquel Barras and too many others to include, as well as the already mentioned Júlio and Nuno. You've been the best company one could wish for during all these years, and I hope to keep you close for as long as possible.

Abstract

The unique proprieties exhibited by nanoscale particles compared to their macro size counterparts allow for the creation of novel neural activity manipulation procedures. In this sense, gold nanoparticles (AuNPs) can be used to stimulate the electrical activity of neuron by converting light into heat.

During this dissertation, AuNPs are synthesized by the citrate reduction method, resulting in a hydrodynamic diameter of approximately 16 nm and an absorbance peak of 530 nm. A system to control a 532 nm laser and measure the temperature variation was custom built from scratch specifically for this project. Temperature is then measured with recourse to a thermocouple and through changes in impedance. The built system had in consideration the necessities presented by in vivo tests.

Trials were performed by measuring the temperature rise of colloidal AuNP solutions, having the temperature variation reached a maximum of approximately 18 $^{\circ}$C relative to control trials; successfully showing that light is effectively transduced into heat when AuNPs are present.

This novel approach enables an alternative to optogenetics, which require the animal to be genetically modified in order to allow neuron stimulation.

Keywords: Gold nanoparticles, neural activity stimulation, optogenetics, plasmonic resonance frequency, photothermal laser heating

Resumo

As propriedades singulares apresentadas pelas partículas à escala nano quando comparadas com as suas contrapartes de tamanho macro permitem que novos procedimentos para a manipulação da atividade neuronal sejam criadas. Neste sentido, nanopartículas de ouro (AuNPs) podem ser utilizadas para estimular a atividade elétrica de neurónios ao converterem luz em calor.

Durante este trabalho, as AuNPs são sintetizadas pelo método de redução de citrato, resultando num diâmetro hidrodinâmico de aproximadamente 16 nm com um pico de absorvância em 530 nm. Um sistema para controlar um laser de 532 nm e medir a variação de temperatura foi construído de raiz especificamente para este trabalho. A temperatura é então medida com recurso a um termopar e através da variação de impedância. O sistema construído teve em consideração as necessidades apresentadas pelos testes in vivo.

Os testes foram efetuados ao medir as mudanças de temperatura apresentadas por soluções coloidais de AuNPs, atingindo estas variações um máximo de aproximadamente 18 °C face a testes controlo, mostrando efetivamente que a luz é convertida em calor na presença de AuNPs.

Esta nova aproximação a este tema possibilita uma alternativa à optogenética, que requer que o animal seja geneticamente modificado de modo a permitir a estimulação neuronal.

Palavras-chave: Nanopartículas de ouro, estimulação de actividade neuronal, optogenética, frequência de ressonância plasmónica, aquecimento fototermal por laser

Index

Index of Figures

Index of Tables

Introduction

1.1.   The Brain

The brain weights just about 2% of our weight, but is a machine of unrivaled mystery and complexity. Composed of approximately 10^{11} base units – neurons, and totaling more than 10^{14} connections between them – synapses; the nervous system effectively builds and processes our perception of the world, of our body, of our feelings and emotions. And yet, with so many progress in other areas of human knowledge this past century (even in respect to the nervous system itself), a full theory regarding the inner workings of the brain is still needed and desired as a major advance in several areas such as biology, medicine, psychology and even computer science.

The neuroscience field has been, for quite a long time, a main interest for not only medical and biological research, but a great range of other seemingly distant fields such as engineering. The unique challenges presented by the study of the brain have, since the first notable discoveries, required a variety of approaches. The fact that neurons and their connections form immensely complex circuits – neural networks, as presented in Figure 1 – develops the requirement for ingenious methods to be able to successfully identify and understand them, as well as the system as a whole.
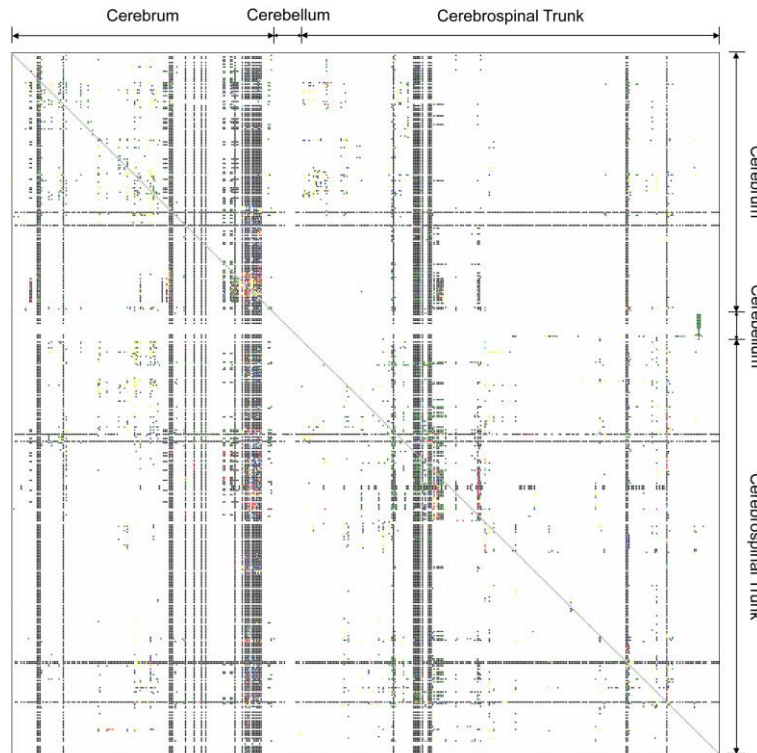
Figure 1 – Matrix displaying curated projection information about sections of the rat brain from several projects. White areas represent areas where information is unavailable, while black areas represent connection absence. The different colors indicate the strength of found projections. The entire matrix is only 10.45% filled, reflecting how little information there is available. Adapted from [1].

Neurons themselves are specialized polarizable cells, capable of integrating and transmitting information. Structurally, a typical neuron consists of the *soma*, or the cell body, inside of which is the nucleus. From the *soma* two different processes arise: several branching dendrites and a single axon elongation, covered with myelin sheaths with regularly placed gaps called nodes of Ranvier, and ending in synaptic terminals (Figure 2).
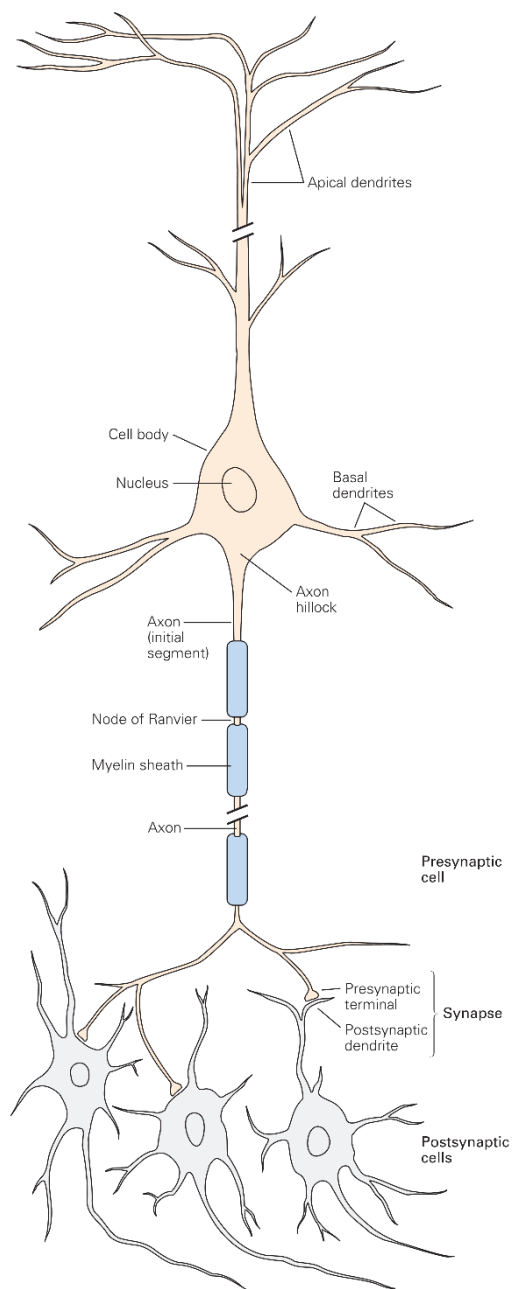
Figure 2 - Representation of a typical neuron and its postsynaptic neighbors. Adapted from [2]**.**

Dendrites serve as the receiving end of inputs for the neuron, while the axon conveys signals to other neurons. These signals – action potentials – are electrical in nature and transmitted due to an electric field between ion concentration present in the intracellular and the extracellular medium. At rest, there is mainly a presence of K^+ and A^- (organic anions) on the inside of the cell, while the outside holds Na^+ and Cl^- ions. Due to the presence of a greater number of ion channels permeable to K^+ and subsequent concentration imbalance, K^+ diffuses through the lipid membrane, resulting in an excess of A^- anions present inside the cell and an excess of K^+ outside; in turn causing a positive extracellular charge in opposition to the negatively charged cytoplasm. This effect is self-limited (since the negative interior results in an inward K^+ flow as well), balanced by the influx of small quantities of Na^+ and Cl^-, and further kept steady by active ion transport through Na^+-K^+ pumps. The resulting resting membrane potential is constant and ranges from -60 to -70 mV relative to the extracellular medium.

When a depolarization event starts occurring and is able to cross the threshold potential, voltage-gated Na^+ channels open and allow a large ion influx into the cell, very rapidly flipping the membrane potential to a positive voltage (+55 mV). This is countered by the closing of Na^+ channels and opening of voltage-gated K^+ channels, returning the resting

13

membrane potential. This brief voltage change propagates forward though the axon, briefly regenerating itself between the myelin sheaths [2]. Figure 3 summarized the events described in the time context of the actual action potential:
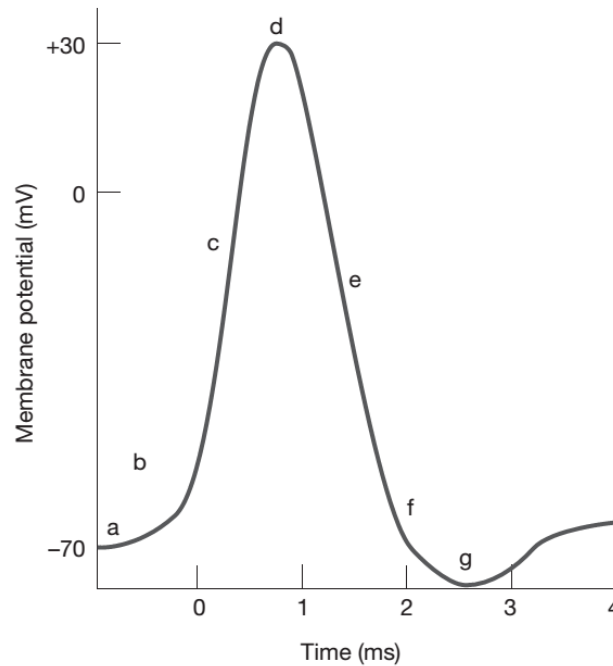
Figure 3 – Representation of a typical action potential signal where (a) represents the resting potential of the cell; (b) is the time the depolarization event starts and membrane permeability to Na+ occurs; (c) at this point both Na+ and K+ channels are open, Na+ rushing into the cell; (d) point at which the Na+ channels close; (e) K+ flows out of the cell; (f) closing of K+ channels; and (g) refractory period. Adapted from [3].

1.2.   *Neural Activity Stimulation*

The advent and evolution of techniques to record or stimulate neurons have been one of the most important driving factors in neuroscience. The discovery and understanding of the complex mechanism behind action potentials, described above, was the basis for the Hogkin-Huxley model and subsequent award of the 1963 Nobel Prize in Physiology or Medicine to their creators, who used the voltage-clamp technique on the axon of a giant squid. [4] Similarly, in 1991 the same prize was awarded to Neher and Sakmann for the development of the patch-clamp technique, which allowed them to further explore single ion channels [5].

14

While a substantial number of new techniques came from the field of microelectronics, such as multi-electrode array (MEA) grids [6], transistor-like structures for neural recording and stimulation [7], high density silicon electrodes with CMOS architecture [8] and flexible electrocorticography (ECoG) grids [9], the approach remains extremely invasive, causing damage to the structures which they stimulate. This damage arises during implantation and from chronic exposure of neural tissue to a foreign material. Many of these devices also require complex preparation and alignment procedures, as well as complicated signal analysis or paired recordings in order to understand the data.

A very recent technique involves the use of light and genetic manipulations in order to stimulate neuronal populations. The first documented use of light to stimulate neurons dates from 1971, when Richard Forks succeeded in using a 488 nm laser beam to excite specific neurons of a marine mollusk, not reaching any clear conclusion on the mechanism which resulted in the observed action potentials [10]. Since then, only in 2005, when neuroscientists developed optogenetics [11], did the dream of successfully and reliably stimulating selected neuronal populations with light became reality. By genetically manipulating a subfamily of light-sensitive proteins designated as channelrhodopsins (ChRs) [12] and expressing it on the neurons of interest, these populations became sensitive to light; since ChRs work as light-gated ion channels (Figure 4).
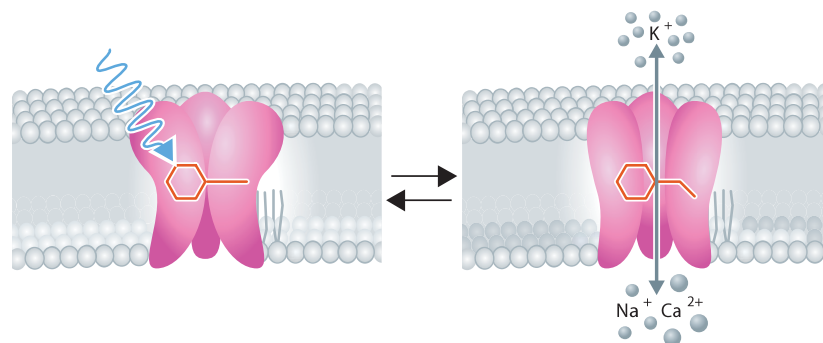
Figure 4 – Representation of channelrhodopsins as light-gated ion channels: incident radiation hits the closed channel in the cell membrane, an isomerization of its covalently bound retinal causes the channel to open, and allows ion flow (and, henceforth, membrane depolarization). Adapted from [13].

While this relatively novel technique has been presenting neuroscience with a substantial amount of new, interesting data, it still presents a few serious drawbacks. The most important of which is the need for genetic manipulation of the subject: this is not possible for every species or neural cell type, and as so, the technique range remains understandably limited.

1.3.   Unmodified-Neuron Optical Stimulation

Due to the problems related to the limitations of genetic modifications required by optogenetics, direct light stimulation of unmodified neurons remained a potential alternative. Allègre et al., in 1994, were able to perform *in vivo* stimulation of a rat nerve bundle with an excimer UV laser [14]. Hirase et al., in 2002, were also able to stimulate unmodified neurons with laser light, this time *in vitro* and using high intensity IR radiation, observing that different sites of the neuron hit by the beam result in a different response [15]. The biophysical mechanisms underlying unmodified neuron stimulation have remained elusive. Shapiro et al. have recently shown that IR laser pulses are absorbed by water, resulting in a local heating effect which briefly increases membrane capacitance and triggers action potential generation [16].

Due to the recent progress with this method, several attempts have been made to improve its results and specificity for targeted neurons. Such approaches have also reaped the benefits of novel advances in micro and nanotechnologies. Lugo et al. tested *in vitro* probes coated with quantum dot (QD) films alongside optical stimulation in order to modulate electrical field potential close to the membrane channels, and elicit depolarization: which is motivated by the similar size of the nanoparticle and the proteins composing the ion channels as well as the possibility of surface modification of the QDs for selective binding [17]. A similar argument can be made for gold nanoparticles (AuNPs), which have recently been used with light of several wavelengths in order to induce the local heating effect described by Shapiro. Several studies [18,19] have reported the use of gold nanorods (AuNRs) stimulated with near infrared (NIR) light in order to provoke depolarization. Carvalho-de-Souza et al. have, in 2015, successfully used

spherically shaped AuNPs functionalized with biological ligands to bind cultured neurons and stimulate them using visible light [20], being the main inspiration of the work developed in this dissertation.

1.4. *Gold Nanoparticle Photothermal Stimulation*

When approaching nano-scale sizes, different types of materials change from their macro-sized counterparts in particular ways: noble metals, such as gold or silver, shift through a variety of colors as particles become smaller in size and with dissimilar shapes. These changes are due to the *collective oscillations of the electron gas*, or surface plasmon (SP) oscillations [21]. Similarly to photons being a quantization of electromagnetic oscillations and phonons a quantization of mechanical oscillations, plasmons arise from variations in the density of free electrons; or the quantization of electron oscillations in the conduction band. Plasmons can become coupled with photons (resulting in a *polariton*) when interacting with resonant electromagnetic radiation. While under surface plasmon resonance (SPR) conditions, colloidal noble metal nanoparticles (such as gold) present a very strong absorption cross-section [22]. This results in a sequence of events: the irradiation of the nanoparticles with resonant radiation induces electron-electron scattering, which causes local heating through the dissipation of phonon interactions with the metal lattice, all in a picosecond timescale with short range heat dissipation [23].

SPR frequency is dependent on the nanoparticle composition, shape, size, orientation and surrounding dielectric environment. Most commonly, gold nanorods exhibit SPR frequencies in the NIR range, while nanospheres of the same material present peaks in absorption spectra close to green visible light [24].

The relative ease of synthesis of gold nanospheres and the high degree of control over the selectivity of the heating effects make these particles considerably good candidates for damage-free photothermal neural cell stimulation.

1.5. *Summary*

Neuroscience has been a field filled with constant evolution and innovation. Deciphering a system as complex as the brain requires the cooperation of several fields and areas of study. Given the electrochemical basis of neuronal signaling,

a wide range of techniques can be employed to both be able to record and manipulate this signal: physical probes, flexible electrocorticography grids, genetic modification and even light in addition to gold nanoparticles, as discussed above. However, while for the last decade nanoparticle heating has been a popular topic in areas such as physics and cancer research, it was seldom applied to neuroscience; and even its effects on the brain were only discovered very recently.

While several *in vitro* articles show AuNP heating to be a promising method, little *in vivo* research has occurred so far using the same applied to cell cultures. Filling that void is the main goal of this research. First, by validating and quantifying the AuNP laser heating effect (Figure 5A), and secondly, by using this knowledge to build a custom setup capable of supplying the same testing conditions for *in vitro* and *in vivo* tests (Figure 5B).
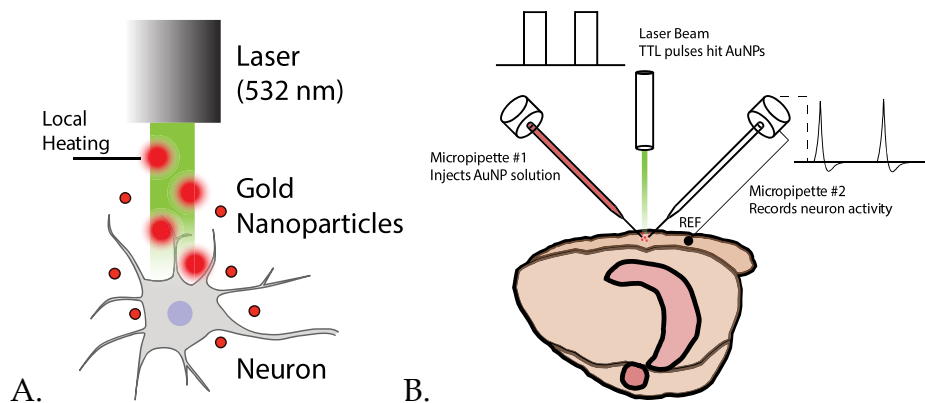
Figure 5 - (A) Schematic representation of AuNP local heating caused by 532 nm light stimulation. Gold nanoparticles in the path of the laser beam are heated due to SPR effects. AuNPs close to the neuron are able to induce action potentials by briefly increasing membrane capacitance. (B) Schematic representation of the setup to be custom built to both record and manipulate action potentials. Both micropipettes are aligned and centered in the same point, to which the laser is aimed. Micropipette #1 is connected to a syringe and injects AuNPs into the extracellular space, which are then heated by TTL-controlled laser pulses. Micropipette #2 is recording neuron activity. Its reference electrode is located in a nearby position in the animal head.

<div align="right">

2

</div>

<div align="right">

Methods

</div>

The materials and methods used during the course of the experiments performed in this dissertation are presented in this section. Gold nanoparticles were synthesized and characterized. A laser setup was used and tuned to test and calibrate the variation of temperature. Finally, a setup (briefly summarized in section 2.4.2 and detailed in section 3.2.2) custom built for *in vivo* surgical procedures was used, detailed in section 2.5.

2.1.   *Synthesis of gold nanoparticles*

Gold nanoparticles were synthesized through the citrate reduction method [25]. 1 mM of tetrachloroauric acid (Sigma-Aldrich, 99.9%) was heated on a hot plate under moderate magnetic stirring until boiling point. 1% (w/v) trisodium citrate (Analar Normapur, 100%) was then added and stirred continuously until the solution turned deep red.

2.2.   *Gold Nanoparticle Characterization*

Characterization of the synthesized gold nanoparticles was performed by two methods: dynamic light scattering (DLS) size measurements and spectrometer measurements of the particle absorbance spectra - given this parameter is essential to verify if the extinction cross-section of the synthesized particles match the laser light frequency.

2.2.1. Dynamic Light Scattering

Hydrodynamic sizes of the produced colloidal nanoparticles were assessed by dynamic light scattering (W130i Avid Nano).

2.2.2. Absorption Spectra

The absorption spectra of the gold nanoparticles was obtained using a spectrometer (PerkinElmer UV/VIS/NIR Spectrometer Lambda 950) with deionized water (Millipore) as baseline.

2.3.   Agar Preparation

Agar gel was prepared by preheating 500 mL of a 1X PBS pH 7.4 solution on a hot plate until boiling. 2.5g of agarose (Próvida, Agar-Agar) were added to the solution and stirred vigorously up to full dissolution. The solution was subsequently poured into several petri dishes and let cool until completely solid.

2.4.   Laser Heating

Gold nanoparticle laser heating tests were performed with two systems. Gold nanoparticles were also tested in solution and in agar gel. Temperature was measured and calibrated using both a thermocouple and the impedance variation of a glass microelectrode.

2.4.1. Optical Fiber Setup (Laser #1)

Laser heating tests were first performed with a 400 mW 532 nm fiber-coupled laser (CNI Optoelectronics, MGL-III-532-400mW) in continuous wave (CW) operation mode. As displayed in Figure 6, the setup consisted of a square sheet of acetate with a circle of black wax printed in the center, two high precision remotely controlled micromanipulators (Scientifica, Patchstar, 61° and Scientifica, IVM, 48.2°), a glass microelectrode, a portable thermocouple (Omega, HH66U), a magnetic mechanical moveable arm (Misumi Corporation, Magnetic Arm) to hold a high definition USB 3.0 camera (PointGrey, Grasshopper). Approximately 0.1 mL of gold nanoparticles or control solution were placed on the center of the wax circle. The glass microelectrode was filled with a 1X PBS pH 7.4 solution, mounted on the right side micromanipulator and slowly descended until the tip

was entirely submerged in liquid. The glass fiber was mounted on the left side micromanipulator, descended without touching the liquid and pointed directly at the glass micropipette tip. On the wax circle, the thermocouple tip and micropipette reference electrode were taped to the surface.
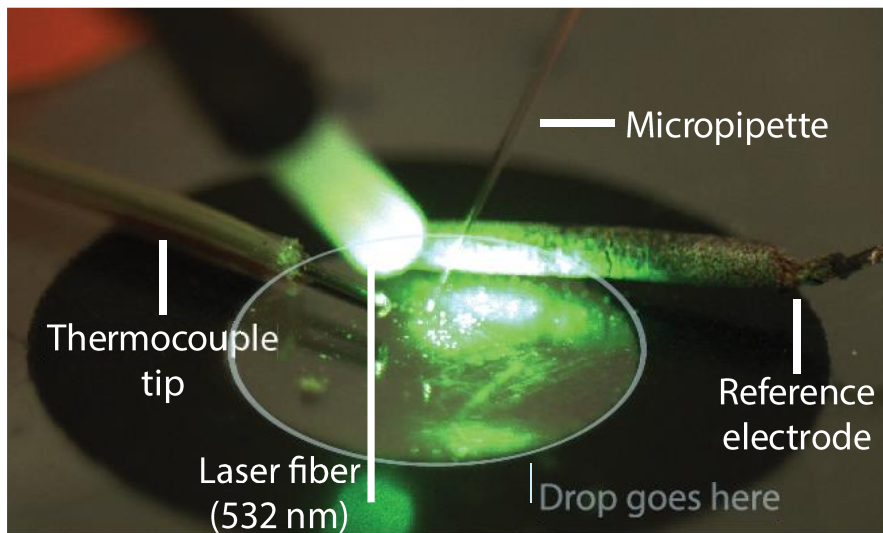
Figure 6 - Annotated photography of the optical fiber setup with the laser turned on. The thermocouple tip and the reference electrode are both placed close to the surface of the wax circle. A drop (either PBS or AuNPs) is then placed in the circle, becoming confined to the inner acetate surface due to wax's hydrophobicity. The micropipette is lowered into the liquid and the tip moved to directly face the laser beam.

2.4.2. Collimated Beam Setup (Laser #2)

A non-fiber-coupled, >150 mW 532 nm DPSS laser (Laserglow, C531505FX) was mounted on a custom built setup and operated in both CW and TTL modes. The setup was assembled on a small support structure and consisted of three interconnected motorized stages (Thorlabs, PT1-Z8).

The structure comprises the laser apparatus pointed directly at a 550nm cutoff longpass dichroic mirror (Thorlabs, DMLP550R) housed at a 45º angle inside a dichroic cage cube (Thorlabs, CM1-DCH). In this cube, two lens tube assemblages (Thorlabs, SM1) were mounted in order to provide video and optical focusing support. In the camera optical path lens tube, a convergent lens (Thorlabs, Convergent Lens f=20cm) and a 600 nm longpass filter (Thorlabs, FEL0600) were screwed between the lens tubes in order to provide focus for the camera and

shielding from green light. TTL pulses were controlled and connected to the laser power source unit through an Arduino board (Arduino LLC, Uno).

Both liquid drop and agarose tests used a setup similar to the one used with the optical fiber test. The laser beam was pointed directly at the glass microelectrode tip using the 3-axis motorized stage assembly. For tests on agarose, a second glass microelectrode was mounted on the left side micromanipulator, filled with gold nanoparticle solution and connected to an air valve; which was plugged in a 5 mL plastic syringe (Terumo, 5ML). This structure was used to inject gold nanoparticles into the testing area. A photography of the setup, with an additional video camera present (Point Grey, Grasshoper), can be seen in Figure 7.
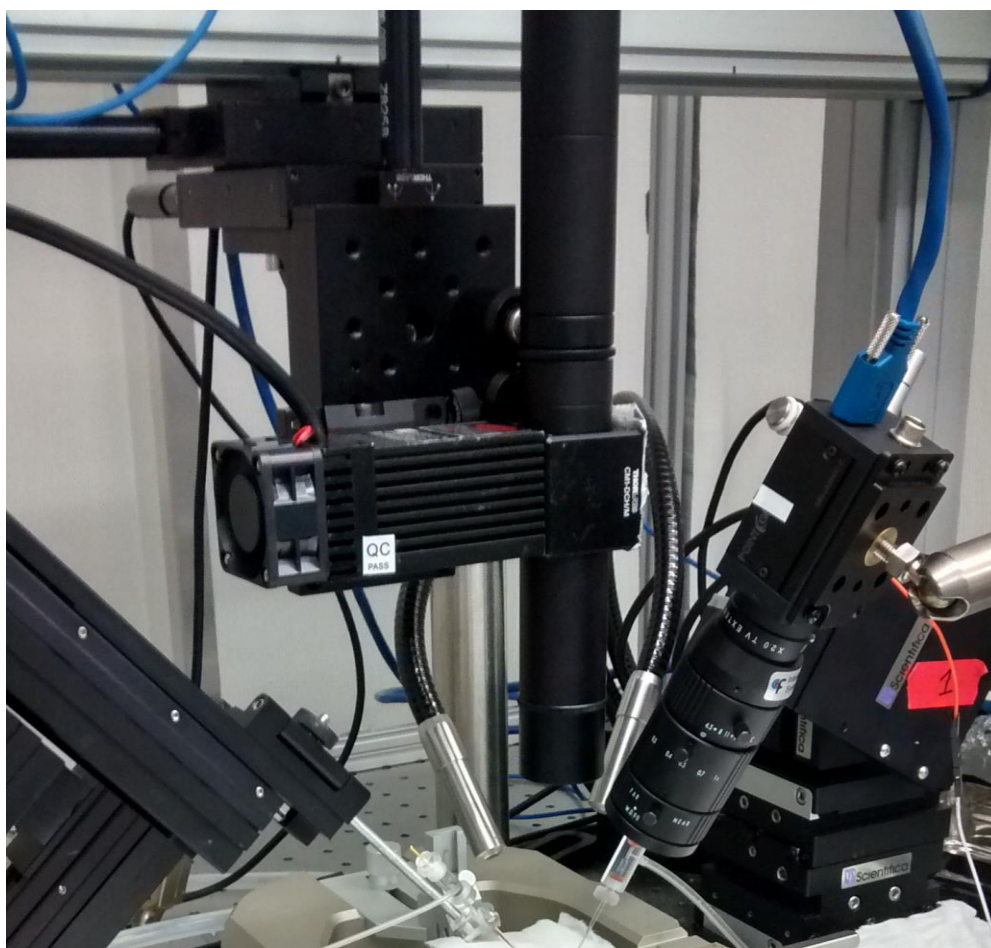
Figure 7 – Image of the custom built Laser #2 setup.

2.4.3. Temperature Calibration

In order to be able to measure changes of temperature in a constrained space, glass micropipettes (tip between 5-10 µm) were used to build a microelectrode and the impedance measured can be then calibrated to temperature [20,26] (Figure 8).

The micropipettes were pulled from 1.5 mm capillary borosilicate glass (Warner Instruments) and filled with PBS 1x. Positive pressure (10-25 mmHg) is maintained in the electrode to keep the tip clear and the amount of pressure and suction applied is monitored through the experiment (DPM1B Pneumatic Transducer Tester, Fluke Biomedical, USA). The amplifier for microelectrode recordings is set in voltage clamp mode and the tip resistance is monitored by observing the current response to steps of voltage of 25 mV, 20Hz (ELC-01X npi, Germany).

This procedure was performed by placing a small petri dish filled with a 1X PBS pH 7.4 solution over a heating pad, with both the thermocouple and microelectrode tips entirely submerged in liquid and placed close to the center. The solution was then heated up to 50°C, and both thermocouple temperature and micropipette impedance were recorded. A calibration curve was then traced and fitted. This equation was then used to calculate the temperatures corresponding to the micropipette impedance signal.
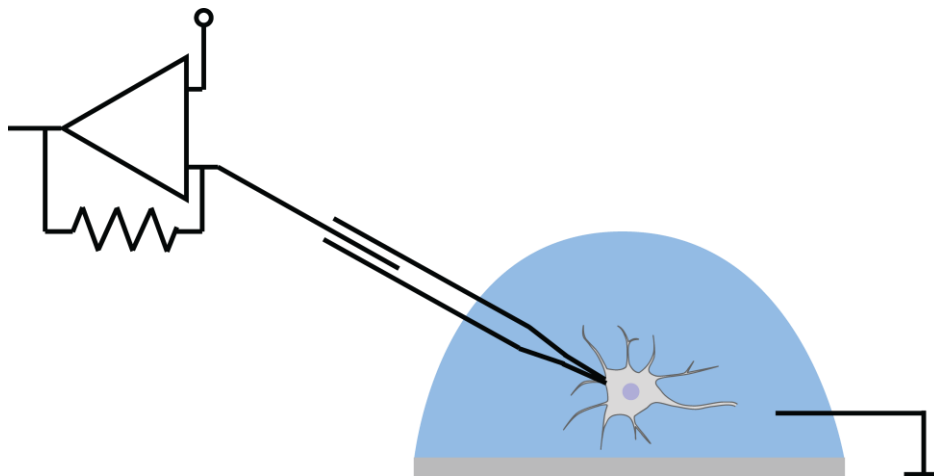
Figure 8 – Diagram of micropipette and microelectrode illustrating how impedance magnitude measurements are obtained.

Results and Analysis

In this chapter results from all the exposed methods will be presented, as well as analyzed and discussed thoroughly. The first section describes the characterization of the gold nanoparticles used in subsequent tests. The second section encompasses the main body of experimental analysis, divided in distinct sections related to the experimental setup in use.

3.1. Gold Nanoparticle Characterization

3.1.1. Particle Size

Gold nanoparticle hydrodynamic diameter was evaluated to be 16.4±0.7 nm using DLS.

3.1.2. Absorbance Spectrum

As seen in Figure 9, the UV-vis spectrograph of the gold nanoparticles shows an absorbance peak (λ_{max}) at 530 nm, which is close to the expected value for the size and shape of synthesized nanoparticles [27]. As the nanoparticle size increases, λ_{max} is red-shifted by a relatively minor amount: $\Delta\lambda$ = 30 nm for 20 to 80 nm nanospheres. This is reported to be due to electromagnetic retardation effects which arise with the increasing size of the particles [28]. Considering devi-

ations from the theoretical value this does not present an issue, as the laser apparatus being used has a wavelength of 532 nm, very close to the measured resonance peak of the synthesized particles.
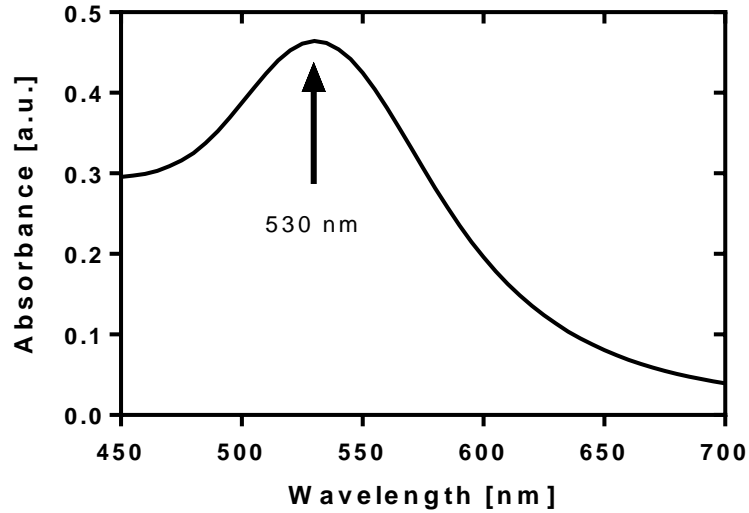
Figure 9 - Observed absorbance spectra of the gold nanoparticles. A peak can be seen at the wavelength of 530 nm.

3.2. *Optical Fiber Setup (Laser #1)*

Laser heating refers to the tests performed regarding the photothermal stimulation of AuNP and control solutions with 532 nm laser light.

3.2.1. *Photothermal Stimulation of AuNP Solution*

In order to assess the validity and reproducibility of local heating of gold nanoparticles, it is first needed to observe how the heating occurs within PBS solution, which, due to similarities to the cerebral-spinal fluid (CSF) is designated as the control; and the gold nanoparticle colloidal solution previously synthesized.

The first tests using the optical fiber setup – Laser #1 (described above on section 2.4.1) - show that both the control solution and the gold nanoparticle solution are affected by the laser light and exhibit a change in temperature (Figure 10A).

The laser beam, while exiting the optical fiber, was measured to have a power of 149 mW. The fiber presented a numerical aperture (NA) value of 0.34, corresponding to a half angle of approximately 20° in air and 26° in PBS (according to the refractive index presented in [29]).

A significant difference in temperature variation can be seen between control and AuNP solutions. Taking into account the temperature measured by the micropipette, the increment was approximately 12 °C and 3 °C, respectively, for the AuNP and control solutions. Micropipette calculated temperatures present higher values, hypothesized to occur due to the measurement precision in the tip (small volume), versus the large volume of liquid measured by the larger thermocouple tip. This is supported by the noticeably lower difference between control measurements in comparison with AuNPs (since control heating is devoid of nanoparticles, heating is expected to be homogenous and hence, similar in both measurement methods, in opposition to the local heating effect expected in the presence of AuNPs). The dissimilar slopes present in the first 20 seconds, measuring 0.34°C/s and 0.09°C/s - corresponding to the micropipette and thermocouple measurements, respectively, are also indicative of a fast short range nanoparticle heating effect such as described in previous literature [20,26]; in comparison with the slower dissipation effect measured by the thermocouple (possibly a diffusion effect).

As seen in Figure 10B, in the presence of an AuNP solution, impedance measured by the micropipette instantly changes when the laser is turned on, exponentially decaying until the laser is turned off. When this occurs, the opposite effect promptly happens, with a rapid exponential growth until almost complete recovery is achieved. Time elapsed between the impedance drop and at least 60% recovery is approximately 20 seconds.
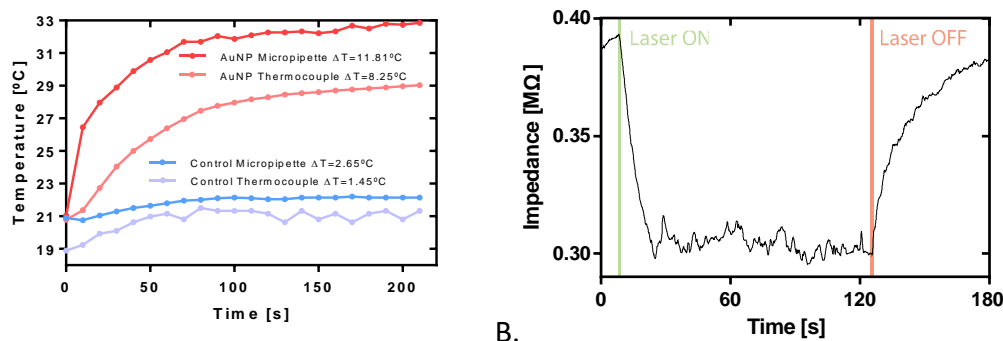
Figure 10 - **(A)** Plot of the several temperature curves observed during the "optical fiber setup" experiment. Results are a collection of mean values between repeated assays. All the data was recovered during a single session so as to use the same glass micropipette. Subsequent calibration for this micropipette yielded a linear relationship through which temperatures were calculated: T = -32,43*Z + 87,77; where T represents temperature (in °C) and Z represents impedance magnitude (in MΩ). **(B)** Example of the effect of laser switching on micropipette impedance profile with an AuNP solution. Both heating and cooling follow exponential curves opposite to each other.

Different AuNP concentrations were tested with the same setup: 25%, 50% and 75% (v/v %). The maximum temperature change is present in the higher concentrations (Figure 11 A and B) Temperature measured with the micropipette is again higher and presents a more distinct difference between the three dilutions, which occurs in approval with the local heating hypothesis previously described. Micropipette heating slopes in the first 20s are seconds are very similar between 50% and 75% dilutions (0.38°C/s and 0.37°C/s, respectively), although lower in the case of the 25% solution (0.28°C/s). Given the similarity between higher concentration results, next tests were performed with a non-diluted AuNP solution unless otherwise noted.
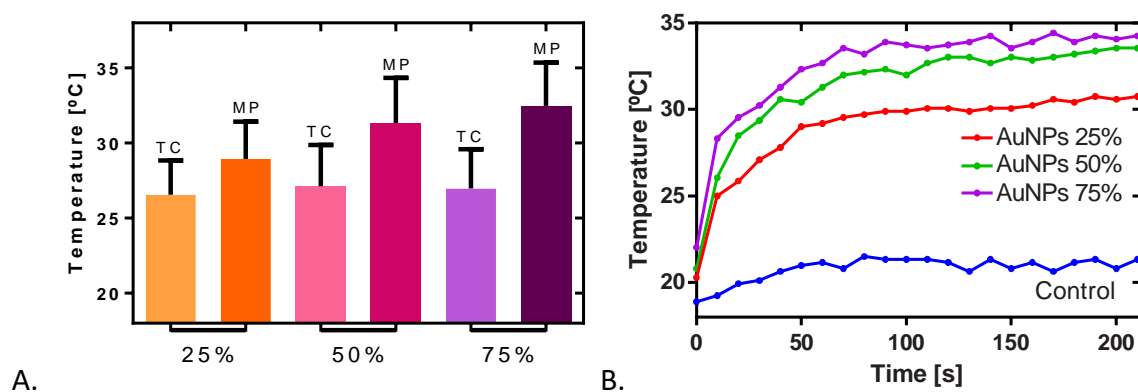
Figure 11 - (A) Comparison of the several AuNP dilutions tested (25%, 50% and 75% v/v %) in order to quantify their effect during photothermal heating. Higher concentrations relate to higher maximum temperatures achieved, in both thermocouple (TC) and micropipette (MP) measurements. (B) Comparison of the micropipette temperature reading of the three dilutions with the control solution along time.

An important factor to consider while working with AuNPs and using the same setup for all the trials is the presence of control contamination. In the results presented, the order of trials was as represented in Figure 12:
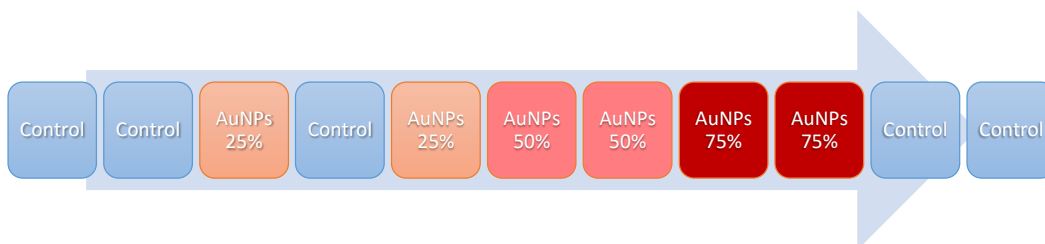
Figure 12 – Diagram representing order of trials performed during the differing dilutions test.

Control trials done after all of the AuNP trials did not show a change in the micropipette results, as seen in Figure 13. While the temperature change reported by the thermocouple is higher than the ones previously observed, the micropipette still shows a similar result. Results are similar, supporting the hypothesis that the micropipette tip is only sensible to local changes, since even if AuNPs are deposited in the surface of the acetate, contributing to the overall heating effect measured by the thermocouple, this effect is not noticeable while in a short volume above the surface.
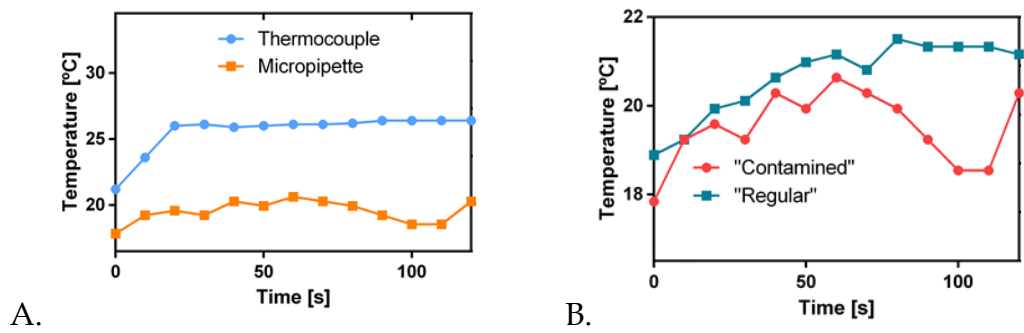
Figure 13 - (A) A "contaminated" control trial with the measured temperatures on the thermocouple and the micropipette. . (B) Comparison between "regular" and "contaminated" trial measured by the micropipette.

3.3.   Collimated Beam Setup (Laser #2)

3.3.1. Laser Setup

A custom laser setup was designed (Figure 14) and built in order to test the next set of both in vitro and in vivo assays. The setup was built taking account spatial constraints due to the surgery and recording rig.
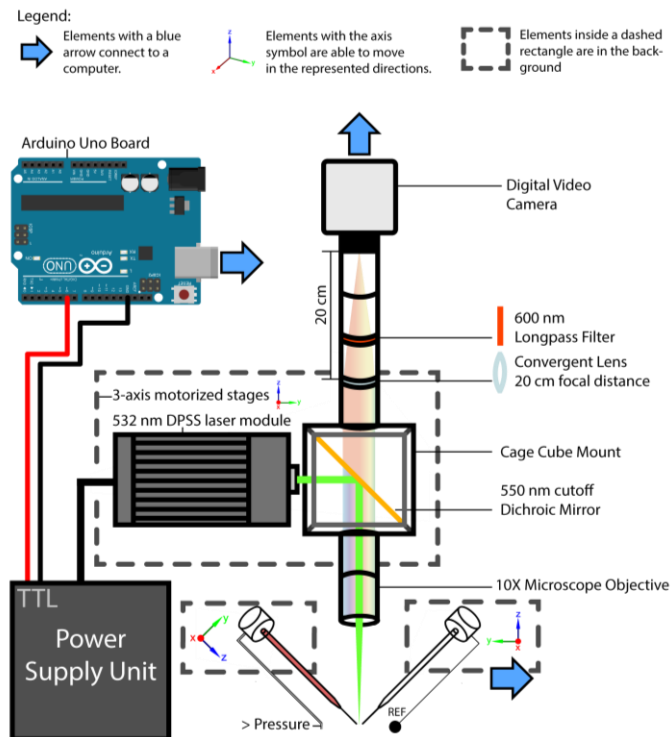
Figure 14 – Schematic representation of the assembled laser setup. Not shown are the elements connected to the right-side micropipette, which can be plugged into the computer

The focusing mechanism works by using the camera as a focus guide for the laser beam and adjusting the Z-axis stage. Since both the light received by the camera and the light emitted by the laser use the microscope objective as a focusing lens, the image received on the screen will be focused at the same time as the laser beam. An image of the described mechanism in an early prototype of the setup is presented in Figure 15:
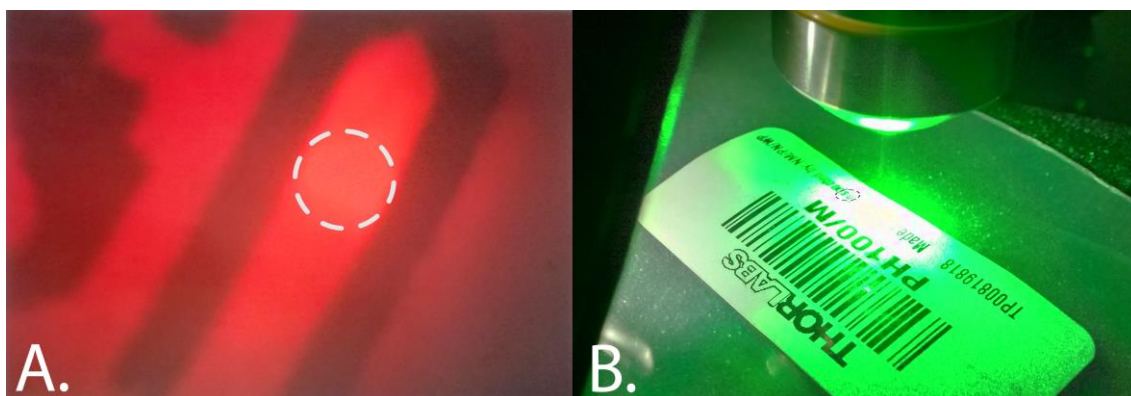
Figure 15 – (A) Live video image from the camera mounted on the top of the setup. Circled is the beam center. (B) Outside view of the setup and of the object being focused. The small circled region shows where the image in A. was focused, as a size comparison.

Three interconnected motorized stages (X-Y-Z directions) are already part of the surgery setup, and both modules are designed to snap into the existing mounts on the Z stage. This makes it possible to assembly the setup during surgery in order to initiate recordings or stimulation.

Laser power in continuous wave mode (CW) was measured to be approximately 245 mW and the beam center size determined to be roughly 700 µm while unfocused and 65 µm when focused with the 10X microscope objective. The beam half-angle was calculated as $0.014 \pm 0.003°$.

3.3.2. *Photothermal Stimulation of AuNP Solution*

In order to assess and validate the use of the new setup in the tests previously performed with the first laser setup, direct heating of both control and AuNP solutions was performed again. Results, as seen in Figure 16, were similar to the ones presented before. A significant difference was again patent between

control and AuNP trials. Maximum temperatures attained were higher, with a ΔT_{Au} of 18.58 °C and a $\Delta T_{Control}$ of 5.83 °C (compared with, respectively 11.81 °C and 2.65 °C from Laser #1). Temperature rise in the first 20 seconds also presents significant differences from previous trials: AuNP solution measures 1.214 °C/s while control measures 0.188 °C/s (compared with 0.34°C/s and 0.09°C/s from Laser #1).
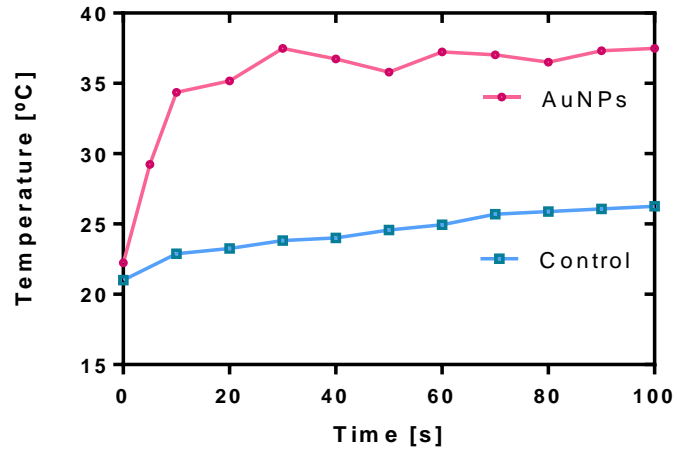
Figure 16 – Photothermal stimulation of AuNPs and control solutions with the new laser setup. Temperature was measured by a calibrated glass micropipette with the tip in the center of the laser beam, following the relationship T = -188.2*Z+89.22.

The rise in temperature variation can be possibly attributed to the increased power in comparison to Laser #1 (116 mW higher), as well as to the smaller spot size yielding higher power per each area unit exposed.

3.3.3. Agar Injection

Following photothermal stimulation of AuNPs and control solutions, the setup was tested with agar. It was chosen due to its similarities with density brain tissue and due to the possibility of localized AuNP injections in the medium. As previously mentioned in Section 2.4.2, these trials were performed using two micropipettes: the first one a microelectrode, dedicated to impedance recording, and the second dedicated to AuNP injection. The recording micropipette is moved slightly into the surface of the agar gel. The injection pipette is loaded with AuNP solution and moved close to the tip from the other pipette (allowing

for an offset in order to avoid collision with the other micropipette) through the guidance of an external magnified video camera feed. Approximately 150 nL of AuNPs are injected into the agar gel following the application of positive pressure.

The injected AuNP solution spreads through the gel as seen in Figure 17. The stained area as measured during several trials, extended for approximately 1 mm across from the injection zone (or more when the surrounding agar presented pronounced valleys, ridges or internal pockets caused by micropipette movement within).
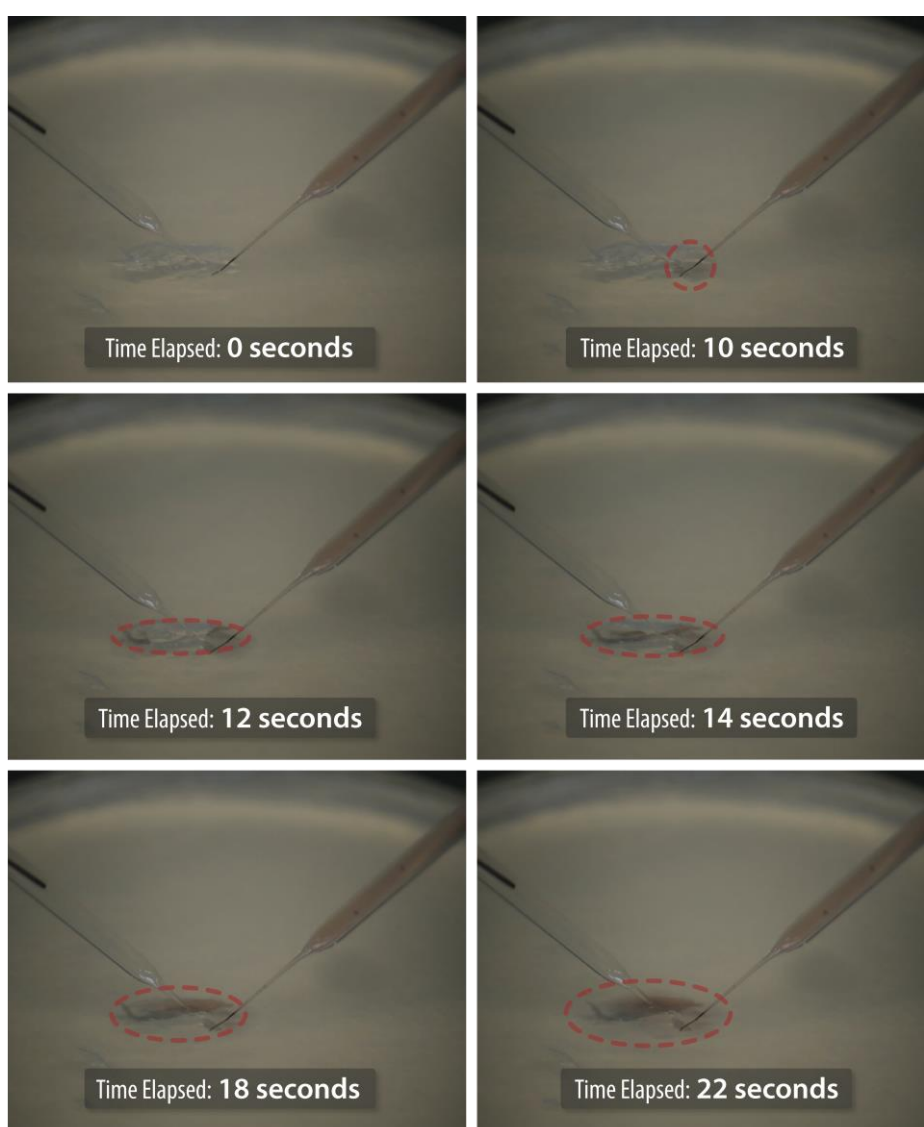
Figure 17 - AuNPs solution injection spreading in agar gel.

3.3.4. Photothermal Stimulation of AuNPs in Agar

AuNP injection in agar was subsequently followed by laser heating. This was done as both a separate and complementary heating trial to the solution tests previously presented, and as a preparation step for an acute surgery scenario, where the same setup would be in use.

In Figure 18 is shown that in the case of AuNPs in agar, a lower maximum temperature is noted, possibly explained by the lower concentration due to the dispersion and diffusion of the AuNP solution across the agar medium.
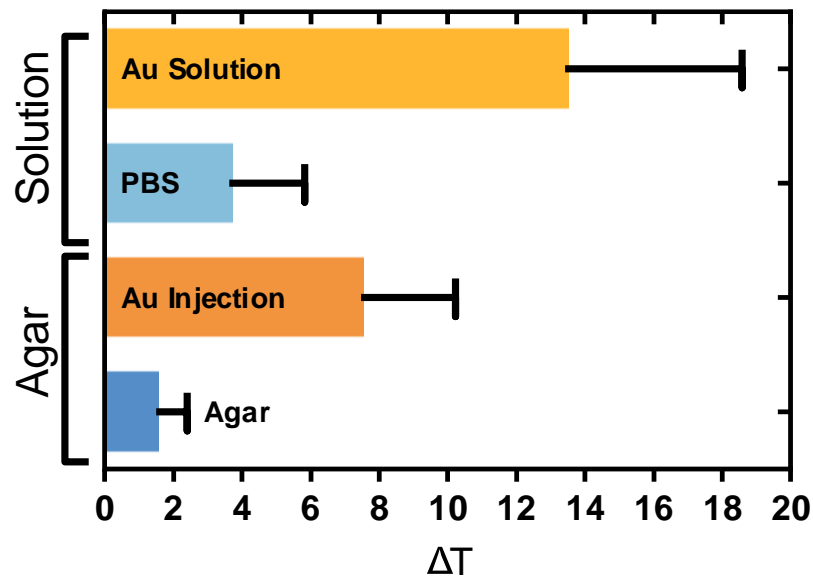
Figure 18 – The mean temperature difference between photothermal stimulation of AuNP in solution and in agar.

While the measurements taken within the visibly stained areas presented very similar measurements colorless (not stained) areas in the gel remained with minute temperature differences, characteristic of typical control reference values.

Therefore, another test performed with the same setup and agar gel consisted of assessing the temperature changes present within several distances of the micropipette tip relative to the laser beam center, as seen in Figure 19.
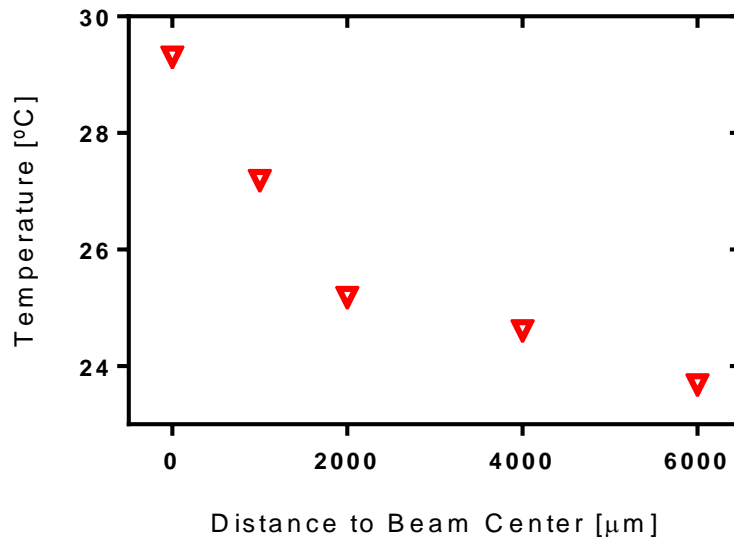
Figure 19 – Temperatures measured with the micropipette electrode at several distances from the beam center. Distances were measured using motor software, and temperatures were calculated following calibration with T = -32.425*Z+77.065.

As expected, temperature tends to increase closer to the center of the beam, corresponding its maximum to 29.3 °C. In contrast, at a distance of 6 mm from the beam center, measured temperatures are close to ambient, at 23.6 °C; meaning a temperature difference $\Delta T = 5.7$ °C between both extremes.

3.3.5. Laser Power

One of the main concerns regarding the laser beam is to ensure sufficient power delivered so as successfully stimulate and penetrate the animal brain tissue in a practical depth profile (considering the laser light penetration depths discussed in the literature [30,31]), without causing significant damage or tissue degeneration.

In order to test beam power and the photothermal effects, different TTL pulses were applied. Symmetrical pulses varying from 1000 Hz to 2 Hz were applied as asymmetrical pulses ranging from 1 ms ON/ 10 ms OFF to 10 ms ON / 500 ms OFF.

Displayed on Table 1 are the measured beam optical powers of the laser setup while the beam is unfocused, in selected pulse modes.

Attempts to reduce the optical power, and, consequently, the damage caused, were performed by applying several symmetrical and asymmetrical TTL pulses to the laser module.

Table 1 - Measured power of unfocused laser beam in selected pulse modes. Temperature increase was measured by directly aiming the beam at the thermocouple tip.

Pulse Type	Continuous Wave	1 kHz	2 Hz	10 Hz	10ms-50ms	10ms-500ms
ΔT (°C)	56	44,4	28,8	28	1,4	0
Power (mW)	265	78,1	101	14,7	2,97	0,4

Selectively, some of these pulse types were then subsequently tested for photothermal stimulation, in order to elicit if a particular pulse can both initiate stimulation of AuNPs while avoiding tissue damage (Table 2).

Table 2 – Tests of selected pulses in agar gel and correspondent maximum temperature variation measured.

Pulse Type	1 kHz	10ms-50ms	10ms-500ms
ΔT Agar (°C)	0.86	0.65	0.88
ΔT AuNPs (°C)	0.95	0.54	0.44

Based on the results presented, no power of the three selected seems to elicit any significant change in temperature in either agar or solution.

The main challenge and question is if is possible to deliver the needed power value (>100mW) to elicit the thermal change in depth without damaging the brain tissue.

4

Conclusions and Future Perspectives

As scientific fields regularly get more interconnected, problems are constantly being conquered through ingenious and novel approaches. One of the most challenging areas remains to be neuroscience, due to the nature and complexity of the systems involved, as well as their micron-scaled size.

Due to recent advances in both the understanding and stimulation of SPR nanoparticle heating and neuron membrane capacitance changes, as well as the benefits of such an activation method compared with natively limited techniques such as optogenetics or physical electrodes – gold nanoparticle neuron stimulation presents itself as an important alternative to study. Given this main motivation, the project presented in this dissertation explored both the validity and quantification of the photothermal heating effects displayed by gold nanoparticles upon SPR laser stimulation.

Gold nanoparticles solution photothermal stimulation trials displayed mean temperature rises approximately 10 $^{\circ}$C greater than the variations measured in PBS solutions. Several dilutions of the gold nanoparticle solution were also tested, revealing a tendency for higher concentrations of AuNPs to be able to attain higher maximum temperature variations. Temperature variation slopes in the first 20 seconds exhibited a large difference between the curve profiles of both solutions upon stimulation: gold nanoparticles presented high slopes (from 0.30 $^{\circ}$C/s in the case of Laser #1 to 1.21 $^{\circ}$C in Laser #2) with an exponential

growth profile, not present in control trials (which had significantly lower slopes, 0.09 °C and 0.12 °C, respectively, in lasers #1 and #2). Temperature values directly measured with the thermocouple probe were also shown to be unreliable in comparison to the temperatures calculated through the calibrated impedance measurements from the microelectrode, possibly due to short-range local heating effects.

In comparison, agar injection tests performed with Laser #2 presented a mean difference of approximately 6 °C between AuNPs and control trials. Both tests lead to the validation of the photothermal heating effect in AuNPs. However, while it occurs and presents itself differently enough from control solutions to be detected, the short range of nanoparticle heating limits accurate measurements by larger, less sensitive devices.

The collimated beam setup (Laser #2) was successfully built, fulfilling its main objective of being able to expand upon the measurements performed with Laser #1. It facilitated the movement of the laser beam, allowed the selective and precise injection of gold nanoparticle solution through the use of a second micropipette - which permitted for the agar injection tests - and changed the laser module - which permitted the application of TTL laser pulses.

Due to the small beam size of Laser #2 it was possible to evaluate temperature changes between different distances from the center of the beam: leading to results showing a temperature difference of roughly 6 °C over a distance of 6 mm from the beam center.

Laser power tests remained as a barrier to further *in vivo* experimentation: their objective was to test and ascertain the effect of several TTL pulses (each resulting in different laser powers) on the photothermal stimulation assay. Exposure of tissue with laser light as powerful as the one measured in both CW and 1 kHz modes has been previously reported to cause lesions [32,33], and, as such, a compromise had to be achieved between the necessary power for AuNP stimulation and the tissue damage threshold. The results presented suggest very little effect from the laser pulses tested on the photothermal heating of AuNPs, which indicates further research is needed in order to successfully find this compromise and be able to perform *in vivo* tests.

In terms of future perspectives, several options are available in order to expand upon the study presented in this dissertation in a number of directions, as well as maneuver the issues encountered. These problems, possible solutions and possible new research opportunities are summarily discussed below.

While the motor-mounted micropipette provides a more reliable and sensitive solution to temperature measurements than the thermocouple probe, it presents several issues:

- They are extremely fragile and must be moved and mounted with extreme care.
- They present different tip sizes and shapes, which display different impedance magnitudes; each requiring a unique calibration in order to calculate temperature values, which is a very time-consuming process.
- Impedance values measured by the microelectrode are extremely sensitive to noise sources and difficult to stabilize.

A possible solution to this problem could be the use of an infrared camera in order to measure temperature changes. The use of such a device has the advantage of offering a spatial view of the data, allowing for more detailed and faster analysis. Furthermore, published work exists successfully employing this method for similar assays [34].

Another problem was the lack of effective regulation of laser power except the use of TTL pulses, which proved unable to effectively stimulate AuNPs. An interesting alternative would be inclusion in the setup of an acousto-optic-modulator (AOM) in order to be able to modify the power delivery in the optical path. Further research with such a device may be able to provide the power compromise required for *in vivo* stimulation.

The potential for the laser powers measured to create tissue damage can be very interesting in fields researching brain lesions. The addition to the setup of a set of galvanometers (as well as the previously mentioned AOM) can allow for very precise, fully automated imprinting of specific lesion patterns in the brain, with varying sizes and depths.

Regarding the research presented by this study itself, important next steps include several paths:

- *In vitro* neural stimulation tests with cultured neurons.
- Further testing of other wavelengths and particles, such as gold nanorods and infrared radiation, or quantum dots.
- Gold nanoparticle surface functionalization in order to allow for effective neuron binding, since the short range heating limits the activation to the membrane surface, close to the temperature-gated channels.
- *In vivo* testing of several beam pulses in order to evaluate tissue damage and stimulation possibilities.
- For further possibilities of *in vivo* tests, use of novel transparent ECoG grids (trECoGs) in order to record neural signals and correlate them with the laser pulses.

Each of these paths provide unique and possibly very important insights into a promising technique which could complement other methods of neural activity stimulation.

5

References

1.   Bohland, J. W. et al. 2009 A proposal for a coordinated effort for the determination of brainwide neuroanatomical connectivity in model organisms at a mesoscopic scale. *PLoS Comput. Biol.* **5**. (doi:10.1371/journal.pcbi.1000334)

2.   Kandel, E. et al. 2012 *Principles of neural science*. 5th edn. McGraw-Hill.

3.   Wickens, A. P. 2014 *A History of the Brain: From Stone Age surgery to modern neuroscience*. 1st Editio. London and New York: Psychology Press.

4.   Hodgkin, A. L. 1964 The Ionic Basis of Nervous Conduction. *Science (80-.).* **145**, 1287–1287. (doi:10.1126/science.145.3638.1287)

5.   Neher, E. & Sakmann, B. 1976 Single-channel currents recorded from membrane of denervated frog muscle fibres. *Nature* **260**, 799–802. (doi:10.1038/260799a0)

6.   Pearce, T. M. & Williams, J. C. 2007 Microtechnology: meet neurobiology. *Lab Chip* **7**, 30–40. (doi:10.1039/b612856b)

7.   Benfenati, V. et al. 2013 A transparent organic transistor structure for bidirectional stimulation and recording of primary neurons. *Nat. Mater.* **12**, 672–80. (doi:10.1038/nmat3630)

8.   Implantable, A. et al. 2013 16.2 An Implantable 455-Active-Electrode 52-Channel CMOS Neural Probe. , 288–290.

9.   Khodagholy, D. et al. 2014 NeuroGrid: recording action potentials from the surface of the brain. *Nat. Neurosci.* **18**, 310–315. (doi:10.1038/nn.3905)

10.   Moscona, a et al. 1969 Laser Stimulation of Nerve Cells in Aplysia Cell-Free Protein Synthesizing System from Yeast Mitochondria. **3**.

11.   Boyden, E. S. et al. 2005 Millisecond-timescale, genetically targeted optical control of neural activity. *Nat. Neurosci.* **8**, 1263–8. (doi:10.1038/nn1525)

12.   Nagel, G. et al. 2002 Channelrhodopsin-1: a light-gated proton channel in green algae. *Science* **296**, 2395–2398. (doi:10.1126/science.1072068)

13.   Hegemann, P. & Nagel, G. 2013 From channelrhodopsins to optogenetics. *EMBO Mol. Med.* **5**, 173–176. (doi:10.1002/emmm.201202387)

14.   Allègre, G. et al. 1994 Stimulation in the rat of a nerve fiber bundle by a short UV pulse from an excimer laser. *Neurosci. Lett.* **180**, 261–264. (doi:10.1016/0304-3940(94)90534-7)

15.   Hirase, H. et al. 2012 Multiphoton stimulation of Neurons and Spines. *Cold Spring Harb. Protoc.* **7**, 472–475. (doi:10.1101/pdb.prot068569)

16.   Shapiro, M. G. et al. 2012 Infrared light excites cells by changing their electrical capacitance. *Nat. Commun.* **3**, 736. (doi:10.1038/ncomms1742)

17.   Lugo, K. et al. 2012 Remote switching of cellular activity and cell signaling using light in conjunction with quantum dots. *Biomed. Opt. Express* **3**, 447. (doi:10.1364/BOE.3.000447)

18.   Eom, K. et al. 2014 Enhanced Infrared Neural Stimulation using Localized Surface Plasmon Resonance of Gold Nanorods. *Small* , 3853–3857. (doi:10.1002/smll.201400599)

19.   Yong, J. et al. 2014 Gold-nanorod-assisted near-infrared stimulation of primary auditory neurons. *Adv. Healthc. Mater.* , 1–7. (doi:10.1002/adhm.201400027)

20.   Carvalho-de-Souza, J. L. et al. 2015 Photosensitivity of Neurons Enabled by Cell-Targeted Gold Nanoparticles. *Neuron* , 1–11. (doi:10.1016/j.neuron.2015.02.033)

21.   Eustis, S. & el-Sayed, M. a 2006 Why gold nanoparticles are more precious than pretty gold: noble metal surface plasmon resonance and its enhancement of the radiative and nonradiative properties of nanocrystals of different shapes. *Chem. Soc. Rev.* **35**, 209–217. (doi:10.1039/b514191e)

22. Huang, X. H. et al. 2006 Cancer cell imaging and photothermal therapy in the near-infrared region by using gold nanorods. *J. Am. Chem. Soc.* **128**, 2115–2120. (doi:10.1021/ja057254a)

23. Roper, D. K. et al. 2007 Microscale heat transfer transduced by surface plasmon resonant gold nanoparticles. *J. Phys. Chem. C* **111**, 3636–3641. (doi:10.1021/jp064341w)

24. Anker, J. N. et al. 2008 Biosensing with plasmonic nanosensors. *Nat. Mater.* **7**, 442–453. (doi:10.1038/nmat2162)

25. Kimling, J. et al. 2006 Turkevich method for gold nanoparticle synthesis revisited. *J. Phys. Chem. B* **110**, 15700–7. (doi:10.1021/jp061667w)

26. Yao, J. et al. 2009 Rapid temperature jump by infrared diode laser irradiation for patch-clamp studies. *Biophys. J.* **96**, 3611–3619. (doi:10.1016/j.bpj.2009.02.016)

27. He, Y. Q. et al. 2005 A study on the sizes and concentrations of gold nanoparticles by spectra of absorption, resonance Rayleigh scattering and resonance non-linear scattering. *Spectrochim. Acta. A. Mol. Biomol. Spectrosc.* **61**, 2861–6. (doi:10.1016/j.saa.2004.10.035)

28. Jain, P. K. et al. 2006 Calculated absorption and scattering properties of gold nanoparticles of different size, shape, and composition: applications in biological imaging and biomedicine. *J. Phys. Chem. B* **110**, 7238–48. (doi:10.1021/jp057170o)

29. Zhernovaya, O. et al. 2011 The refractive index of human hemoglobin in the visible range. *Phys. Med. Biol.* **56**, 4013–21. (doi:10.1088/0031-9155/56/13/017)

30. Yizhar, O. et al. 2011 Optogenetics in neural systems. *Neuron* **71**, 9–34. (doi:10.1016/j.neuron.2011.06.004)

31. Huber, D. et al. 2008 Sparse optical microstimulation in barrel cortex drives learned behaviour in freely moving mice. *Nature* **451**, 61–4. (doi:10.1038/nature06445)

32. Sramek, C. et al. 2011 Non-damaging Retinal Phototherapy: Dynamic Range of Heat Shock Protein Expression. *Investig. Opthalmology Vis. Sci.* **52**, 1780. (doi:10.1167/iovs.10-5917)

33.	Jackson, J. et al. 2015 Laser-Mediated Microlesions in Mouse Neocortex to Investigate Neuronal Degeneration and Regeneration. *Curr. Protoc. Neurosci.* , 2.24.1–2.24.17. (doi:10.1002/0471142301.ns0224s73)

34.	Kojic, N. et al. 2012 Focal Infection Treatment using Laser-Mediated Heating of Injectable Silk Hydrogels with Gold Nanoparticles. *Adv. Funct. Mater.* **22**, 3793–3798. (doi:10.1002/adfm.201200382)
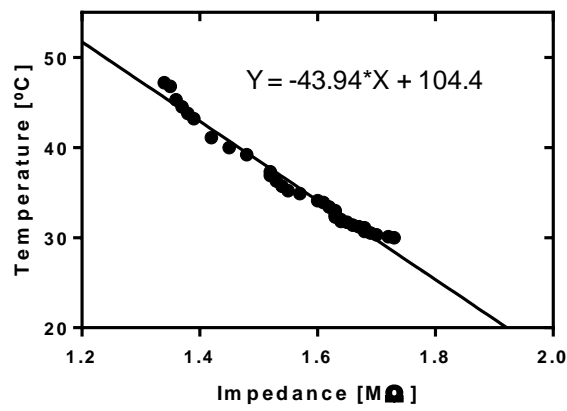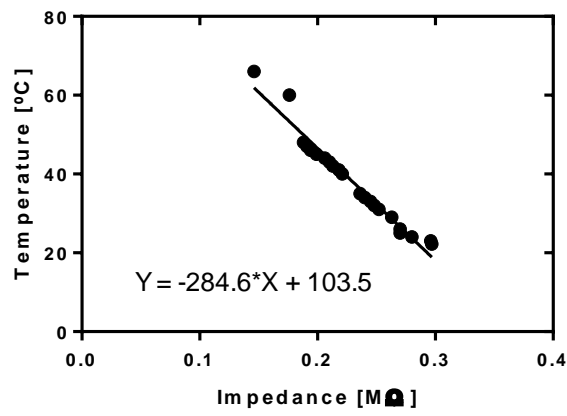
6

Appendix

Section A

Calibration Curves

$$Y = -188.2*X + 89.22$$

$$Y = -24.06*X + 108.9$$
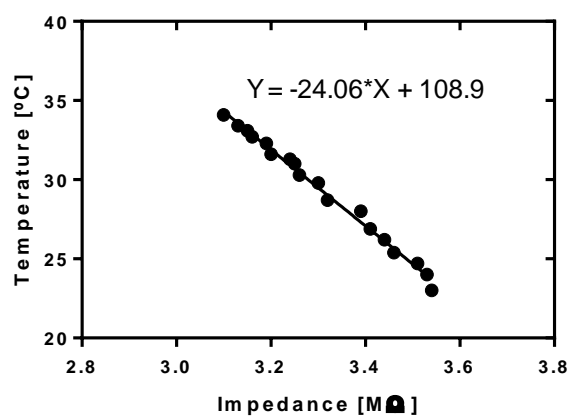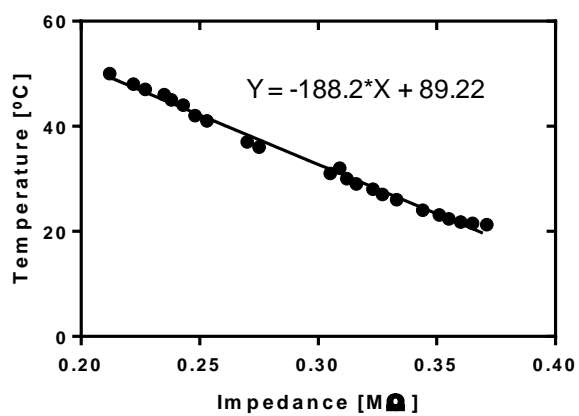
Figure 20 – Calibration curves used to convert impedance measurements from the microelectrode into temperature.

Section B

Arduino Code used for TTL pulses

```
int outPin = 6;
//int freq = 1000; //Enter frequency in Hz
//int period = (1/freq)*1000;

void setup() {
  pinMode(outPin, OUTPUT);
  Serial.begin(9600);
}

void loop() {
  digitalWrite(outPin, HIGH);
  Serial.print("LOW \n");
  delay(500); // Set pulse pause time in miliseconds
  digitalWrite(outPin, LOW);
  Serial.print("HIGH \n");
  delay(500); // Set pulse time in miliseconds
}
```
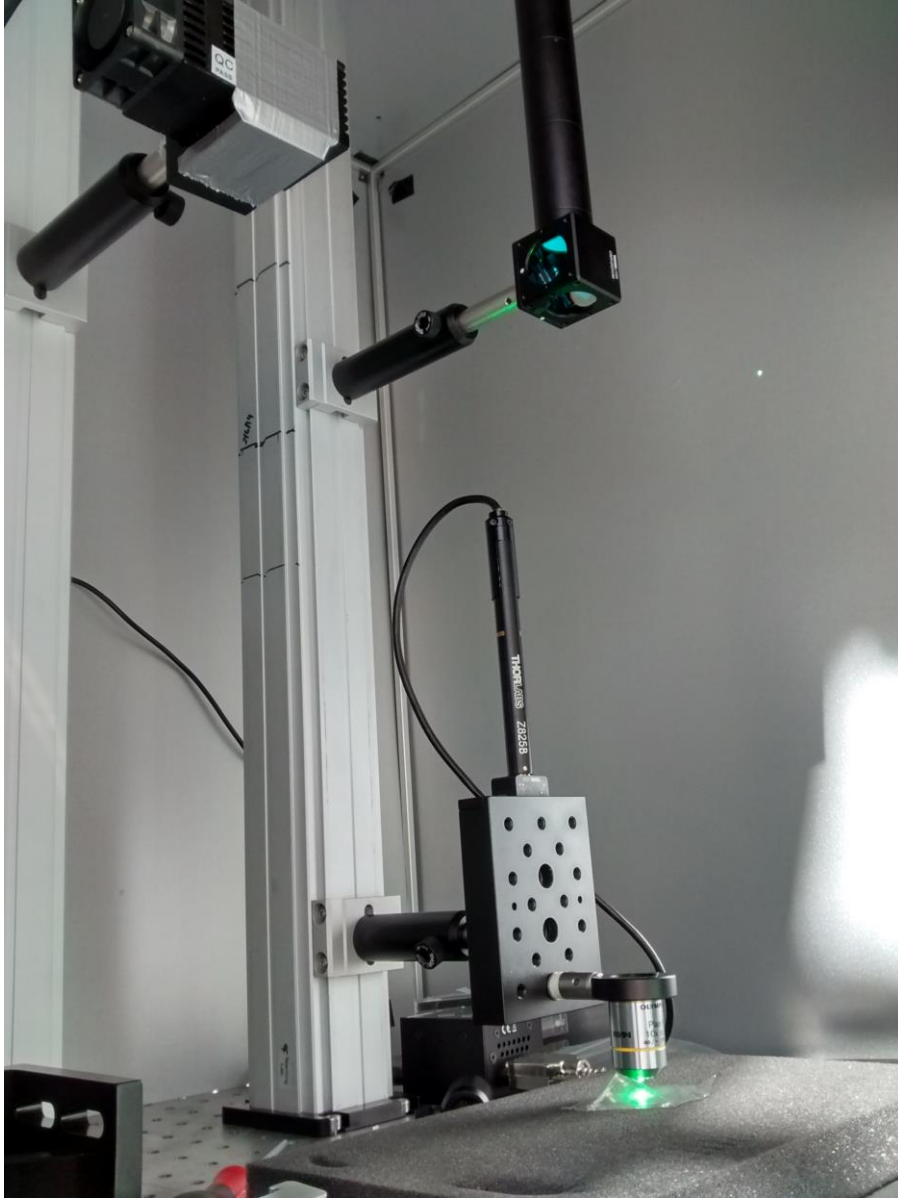
Section C

Images of Laser #2 Setup Prototyping

Figure 21 – Photograph of early structure depicting laser module aimed at the dichroic mirror after assembly.

Figure 22 – Laser setup prototype with all parts assembled and small microscope lens, without portability.
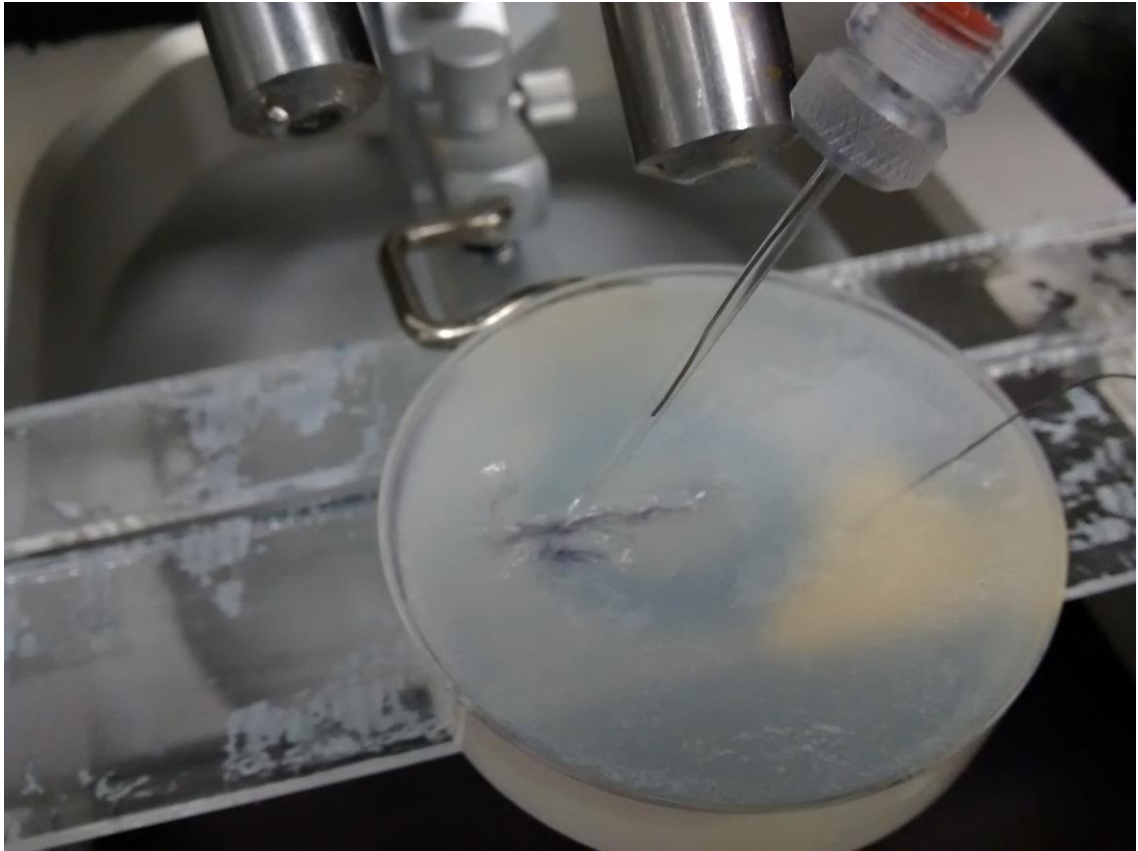
Figure 23 – Impedance measuring on agar gel after AuNP injection.